A&A 482, 387–395 (2008)
DOI: 10.1051/0004-6361:20079300
© ESO 2008

Astronomy & Astrophysics

The FeH $F^4\Delta$–$X^4\Delta$ system

Creating a valuable diagnostic tool to explore solar and stellar magnetic fields

N. Afram[1], S. V. Berdyugina[1,2], D. M. Fluri[1], S. K. Solanki[3], and A. Lagg[3]

[1] Institute of Astronomy, ETH Zurich, 8092 Zurich, Switzerland
e-mail: nafram@astro.phys.ethz.ch
[2] Tuorla Observatory, University of Turku, 21500 Piikkiö, Finland
[3] Max-Planck-Institut für Sonnensystemforschung, Max-Planck-Strasse 2, 37191 Katlenburg-Lindau, Germany

Received 21 December 2007 / Accepted 16 January 2008

ABSTRACT

Context. Lines of diatomic molecules are ideal tools for studying cool stellar atmospheres and the internal structure of sunspots and starspots, given their temperature and pressure sensitivities, which are typically higher than in atomic lines. The Wing-Ford FeH $F^4\Delta$–$X^4\Delta$ system represents such a diatomic molecule that is, in addition, highly sensitive to magnetic fields. The current theoretical description of those transitions that include the involved molecular constants, however, are only based on intensity measurements because polarimetric observations have not been available until now, which limits their diagnostic value. Furthermore, the theory has so far been optimized to reproduce energy levels and line strengths without taking magnetic sensitivities into account.
Aims. The FeH $F^4\Delta$–$X^4\Delta$ system is produced by transitions between two electronic states with the coupling of the angular momenta that is intermediate between limiting Hund's cases (a) and (b). Our goal is to investigate the diagnostic capabilities of the current theoretical description of the molecule FeH.
Methods. Using the most precise available Hamiltonian, we carried out the perturbation calculation of the molecular Zeeman effect for this transition and computed the Landé factors of the energy levels and of transitions. We extracted Landé factors from a comparison of observed and calculated Stokes I and V profiles. Certain spectral lines, most frequently with high magnetic sensitivity, exhibited discrepancies between the theory and observations. We extended the theoretical model with a semi-empirical approach to obtain a diagnostic tool that is able to reproduce many of the interesting spectral lines.
Results. We find that the current theory successfully reproduces the magnetic properties of a large number of lines in the FeH $F^4\Delta$–$X^4\Delta$ system and that the modified Hamiltonian allows us to synthesize and successfully reproduce the most sensitive lines. Thus, our observations have provided valuable constraints for determining empirical molecular constants and Landé factors.
Conclusions. The FeH $F^4\Delta$–$X^4\Delta$ system is found to be a very sensitive magnetic diagnostic tool. Polarimetric data of these lines, in contrast to intensity measurements, provide us with more direct and detailed information to study the coolest parts of sunspot and starspot umbrae, as well as cool active dwarfs.

Key words. molecular processes – Sun: magnetic fields – polarization – radiative transfer – line: formation – stars: magnetic fields

1. Introduction

The potential of molecular spectropolarimetry for the study of solar and stellar magnetic fields has become evident over the past years. An overview of the magnetic properties of molecules observed in spectra of sunspots and cool stars was given by Berdyugina et al. (2000, 2003), where they showed the usefulness of lines of astrophysically important diatomic molecules as indicators of the physical parameters prevalent in a sunspot, including magnetic field strengths. Iron hydride (FeH) is one of the most sensitive indicators of magnetic fields in cool atmospheres. Zeeman-broadened FeH lines in an active M dwarf were detected by Valenti et al. (2001), showing the usefulness of the FeH lines as stellar magnetic field diagnostics. Because of the lack of a theoretical description of the FeH molecule, they modeled the stellar spectrum employing the sunspot measurements by Wallace et al. (1998). First modeling of synthetic Stokes profiles of FeH lines indicated that the FeH $F^4\Delta$–$X^4\Delta$ system represents a powerful tool for diagnosing solar and stellar magnetism once the spin-coupling constants are available (Berdyugina et al. 2001, 2003).

Dulick et al. (2003, hereafter Dea03) provided the necessary set of the missing molecular constants. In particular, they determined the spin-orbit (A) and spin-spin (λ) constants for the FeH $F^4\Delta$–$X^4\Delta$ system, using the laboratory spin-splitting data from Phillips et al. (1987). They found that the spin splittings for the observed vibrational levels could be reproduced within an error of 0.5 cm^{-1} by a single pair of A and λ values for each electronic state for a given parity. However, the achieved accuracy was still a factor of 10 lower than the experimental uncertainties, indicating perturbations that had not been accounted for. Nevertheless, the analysis by Dea03 promises to advance our understanding of the magnetic properties of FeH lines. Recently, Afram et al. (2007) have reported first polarimetric measurements of this FeH system and gave examples of both the applicability and the failures of the current theory.

In this paper we address the limitations of the available set of molecular constants in detail and offer a semi-empirical solution to the problem. For this work we analyzed datasets from various observations, which are specified in Sect. 2. In Sect. 3 the description of the molecular Zeeman effect in the FeH $F^4\Delta$–$X^4\Delta$ system is given. In Sect. 4, molecular line profiles in the

presence of magnetic fields in the Zeeman regime are calculated, using the theory presented in the previous section. A comparison of the synthetic Stokes profiles with profiles observed in sunspots is presented (Sect. 4.1). We then discuss the deficiencies of the theoretical model based on using the molecular constants by Dea03 and describe our semi-empirical model to account for unknown perturbations in the theory (Sect. 4.2). With the help of our sunspot observations, we determined the Landé factors of the energy levels and the Landé factors of transitions and compared both the calculated and observed effective Landé factors in Sect. 5. In contrast to laboratory measurements, the Landé factors of the energy levels can be determined not only for low rotational numbers in the ground state, but also for high rotational numbers and also for the excited state. In Sect. 6, we briefly discuss the importance of FeH for diagnosing magnetic fields in brown dwarfs, where atomic lines vanish due to colder temperatures.

2. Sunspot data

Before going into our own synthetic spectra, we first outline the measurements of sunspots by different authors.

Rüedi et al. (1995) presented observations made on 30–31 January 1991 with the McMath-Pierce solar telescope on Kitt peak and the Fourier transform spectrometer (FTS) combined with a polarimeter. The data used were taken in the darkest part of a sunspot umbra (member of the group NOAA 6469) and contain intensity and polarization measurements of the (0, 1) band of the FeH $F^4\Delta$–$X^4\Delta$ system around 12 000 Å. Using the splitting of Fe lines, we determined a magnetic field strength of 2.8 kG. The direction of the magnetic field vector was aligned along the line of sight, pointing towards the observer.

Wallace et al. (1998) published an umbral spectrum obtained with the the Brault Fourier transform spectrometer (FTS) on 9 August 1981. Using the splitting of three Ti lines, they determined a magnetic field strength of 2.7 kG for this dataset. Although polarimetric measurements were not contained in their observations, we used their spectra to obtain fits to the intensity profiles of the FeH (0, 0) band of the $F^4\Delta$–$X^4\Delta$ system around 10 000 Å, which show significant Zeeman pattern broadening. The measurements of the Zeeman pattern widths presented in their work show for the different branches how the splitting depends on the J number. We investigate this behavior in Sect. 5.2.

An additional set of data was obtained with the polarimeter TIP (Mártinez Pillet et al. 1999) (mounted behind the Echelle spectrograph at the VTT) on Tenerife. On 22 May 2001, measurements were made in sunspot NOAA 9462. A wavelength interval of about 7 Å was observed around 10 422 Å. The exposure time for each slit position (scanning mode) was 0.05 s for each Stokes parameter. A complete cycle of Stokes vector observations required 120 accumulations and resulted in a total exposure time of 24 s for each image. The *S/N* ratio was around 2000. Using the splitting of Fe lines, a magnetic field strength of 3 kG was determined. The direction of the magnetic field vector was aligned along the line of sight, pointing towards the observer.

Afram et al. (2007) presented polarimetric data for a sunspot (NOAA 0663) measured at Istituto Ricerche Solari Locarno (IRSOL) with the 45 cm aperture Gregory Coudé telescope and a two-beam exchange polarimeter on 23 August 2004. To observe lines of the (0, 0) band of the FeH $F^4\Delta$–$X^4\Delta$ system in the near infrared, they used the original Semel polarimeter. A magnetic field strength of 3 kG was determined from atomic lines, and the magnetic field vector was aligned along the line of sight, pointing away from the observer.

3. The molecular Zeeman effect

If a molecule possesses a nonzero magnetic moment, it interacts with an external magnetic field and causes a precession of the total angular momentum J about the field direction. As a result one can observe the Zeeman effect, i.e. the magnetic splitting of energy levels in the molecule. The largest contribution to the magnetic moment of a diatomic molecule comes from the magnetic moment associated with the orbital and spin angular momenta of electrons, $\boldsymbol{L}$ and $\boldsymbol{S}$, respectively, i.e.

$$\mu = \mu_L + \mu_S = \mu_0(\boldsymbol{L} + 2\boldsymbol{S}), \tag{1}$$

where μ_0 is the Bohr magneton ($\mu_0 = \frac{eh}{4\pi mc}$, with the electron charge e and mass m). If these moments are zero, the contributions from the rotational motion of the molecule and the spins of the nuclei must be taken into account.

The energy of the interaction of the magnetic moment μ with the external field $\boldsymbol{H}$ is given by

$$\Delta E = -\mu\boldsymbol{H} = -\mu_0(\boldsymbol{L} + 2\boldsymbol{S})\boldsymbol{H} = g\Delta\sigma_0 M, \tag{2}$$

where g is the level Landé factor and $\Delta\sigma_0 = \mu_0 H$. The energies of magnetic components depend on how the angular momenta are coupled with each other and to the rotation of the molecule.

3.1. Zeeman effect in Hund's case (a–b): FeH

The FeH $F^4\Delta$–$X^4\Delta$ system is produced by transitions between two electronic quartet states with $\Omega = \frac{7}{2}, \frac{5}{2}, \frac{3}{2}$, and $\frac{1}{2}$, Ω being the quantum number for the component of the total electronic angular momentum along the internuclear axis of a diatomic molecule. The coupling of the angular momenta is intermediate between limiting Hund's cases (a) and (b). The perturbation calculation of the molecular Zeeman effect is based on the effective Hamiltonian for this transition, which can be presented by two parts, $\mathcal{H}^{\rm ab}$ and $\mathcal{H}^{\rm H}$:

$$\mathcal{H} = \mathcal{H}^{\rm ab} + \mathcal{H}^{\rm H}, \tag{3}$$

the former performing the transformation of the case (a) wavefunctions $\Psi^{\rm a}$ into the intermediate wavefunctions $\Psi^{\rm ab}$ and the latter describing the interaction with the external magnetic field.

The matrix elements of the Hamiltonian $\mathcal{H}^{\rm ab}$ determining the spin-orbital, spin-spin, rotational, and centrifugal distortion interactions in the electronic state described with Hund's case (a) wavefunctions as a basis set are given in Dea03.

The effect of the external magnetic field is described by the matrix elements of the perturbation $\mathcal{H}^{\rm H}$:

$$\mathcal{H}^{\rm H}(\Lambda,\Sigma;\Lambda,\Sigma) = \frac{(\Lambda+2\Sigma)\Omega}{J(J+1)} M\Delta\sigma_0, \tag{4}$$

$$\mathcal{H}^{\rm H}(\Lambda,\Sigma;\Lambda,\Sigma\pm1) = \frac{M\Delta\sigma_0}{J(J+1)} \times \sqrt{S(S+1)-\Sigma(\Sigma\pm1)} \times \sqrt{J(J+1)-\Omega(\Omega\pm1)}. \tag{5}$$

By diagonalization of the total Hamiltonian $\mathcal{H} = \mathcal{H}^{\rm ab} + \mathcal{H}^{\rm H}$ (Berdyugina et al. 2005), we obtain the energy levels of the magnetically perturbed system and thus the Zeeman shifts ΔE_N of the energy levels with $N = 0, 1, 2, 3$ for the examined FeH system. We denote rotational branches with indices 1, 2, 3, and

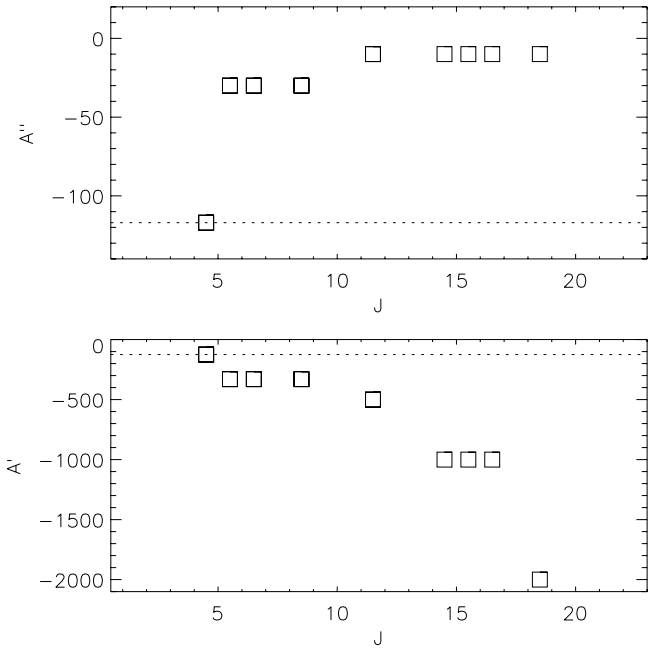

Fig. 1. Spin-orbit constants A'' and A' for lower and upper electronic states, respectively, as functions of the J number for the P_4 branch. The dotted lines indicate the values by Dea03, which are the same for all J.

4 as corresponding to transitions between levels, both having $\Omega = 1/2, 3/2, 5/2, 7/2$.

Together with molecular constants for the FeH $F^4\Delta$–$X^4\Delta$ system provided by Dea03, the diagonalization of the Hamiltonian leads to satisfying results for many spectral lines (see Sect. 4.1). However, our spectral synthesis reveals that the Hamiltonian provided by Dea03 does not sufficiently account for perturbations in lines of certain branches with higher rotational numbers. For those lines we carried out an analysis to find an empirical set of molecular constants to fit the observed spectral line (Sect. 4.2). Thus, we obtained the Landé factors for each of the perturbed lines, which allows a description of those lines without the knowledge of the accurate molecular constants. The theoretical line strengths were calculated with the constants by Dea03. Finally, note that we have not distinguished the parity of levels in our calculations, since the difference in their magnetic sensitivity is beyond our measurement accuracy.

4. Stokes profiles in the Zeeman regime

Implementing the Hamiltonian given in Eq. (3), we can now calculate molecular Stokes profiles in the presence of magnetic fields in the Zeeman regime, using the code STOPRO (Solanki 1987; Solanki et al. 1992; Frutiger et al. 2000; Berdyugina et al. 2003, 2005). The synthetic Stokes profiles are compared with those observed in sunspots. We first obtain best fits to Stokes profiles of lines with negligible perturbations, i.e. those transitions that are described well by the model of Dea03. For this purpose we vary only the effective temperature of the model atmosphere while fixing the magnetic field strength and direction to the values determined from atomic lines (Sect. 4.1). In a second step, we obtain best fits to Stokes profiles of those transitions that suffer from unknown perturbations by varying the spin-orbit interaction constants and keeping the magnetic fields fixed for a given sunspot (Sect. 4.2).

Atmosphere models are from Hauschildt et al. (1999). To account for the stray light from the photosphere, we combined calculated sunspot and photospheric spectra using various spot filling factors. We notice that the temperature model had to be different for the same spot, indicating inaccurate line strengths and introducing an unknown bias to uncertainties in temperatures and filling factors. However, the magnetic field analysis is not affected by this issue, which will be analyzed in our next studies.

Our final goal, however, was not to determine the accurate spin-orbit constants for the FeH $F^4\Delta$–$X^4\Delta$ system, but to extract the best-fit Landé factors of the levels and transitions for each spectral line depending on the Ω and J numbers. Previous calculations (see Berdyugina & Solanki 2002), show that the highest magnetic sensitivity for Hund's case (a–b) was reached if one state is in Hund's case (a) and the other in Hund's case (b), which results in an increase in the magnetic sensitivity with increasing rotational number J. Measurements by Wallace et al. (1998) indicate this behavior for FeH transitions. We find that this could be reproduced by increasing the spin-orbit constant of the lower level (A'') and decreasing the spin-orbit constant of the upper level (A') in comparison to the values given by Dea03. Such a change imposes the lower level being closer to Hund's case (b) and the upper one closer to Hund's case (a). An example of this behavior is shown in Fig. 1 for lines of the P_4 branch. With the opposite adjustment, i.e. when decreasing A'' and increasing A', the fits cannot be achieved. It is obvious that adjusting the spin-orbit constant does not lead to their accurate values, which must be found in a laboratory analysis, but it can be employed as a tool for obtaining Landé factors of levels and transitions. These can be used in the future as input for finding a more accurate Hamiltonian describing this system. On the other hand, the uncertainties in the model parameters and different line formation depths limit the accuracy of the determined molecular constants and Landé factors.

Below we describe the fits to the Stokes profiles observed in sunspots. The best-fit solutions provide us with the estimates of the Landé factors of both levels and transitions. In the following they are called best-fit Landé factors, whereas the Landé factors obtained from polynomial expansions are called approximated Landé factors, for the sake of clarity. They are discussed further in Sect. 5.

4.1. Unperturbed transitions

With the molecular constants from Dea03, many spectral line profiles of the (0, 0) band with various ΔJ, J, and Ω can be reproduced. Lines of the Q-branch with $J \leq 4.5$ exhibit particularly strong magnetic sensitivity as was expected from earlier investigations (Berdyugina & Solanki 2002). Also the P and R lines with $\Omega \lesssim 2.5$ and $J \lesssim 10.5$ can be properly modeled (see Figs. 1 and 2 in Afram et al. 2007).

In Fig. 2 we present synthetic Stokes I (upper panels) and V (lower panels) profiles compared with the observed spectra (only Stokes I) from Wallace et al. (1998). Perturbations seem to be less important in lines of the Q-branch ($\Delta J = 0$) where the J number is the same in the lower and upper levels and thus perturbations seem to operate in the same way and cancel out. For the P- and R-branches, such cancelations do not occur and perturbations become a major issue in P- and R-lines with high $\Omega \geq 3.5$ and $J \gtrsim 10.5$. However, for the P- and R-branches and $\Omega \lesssim 2.5$ and $J \lesssim 10.5$, a good range of spectral lines can be reproduced synthetically with the molecular constants from Dea03 as can be seen in Fig. 2. It seems that for higher J and higher Ω, those constants are not adequate any longer, since perturbations

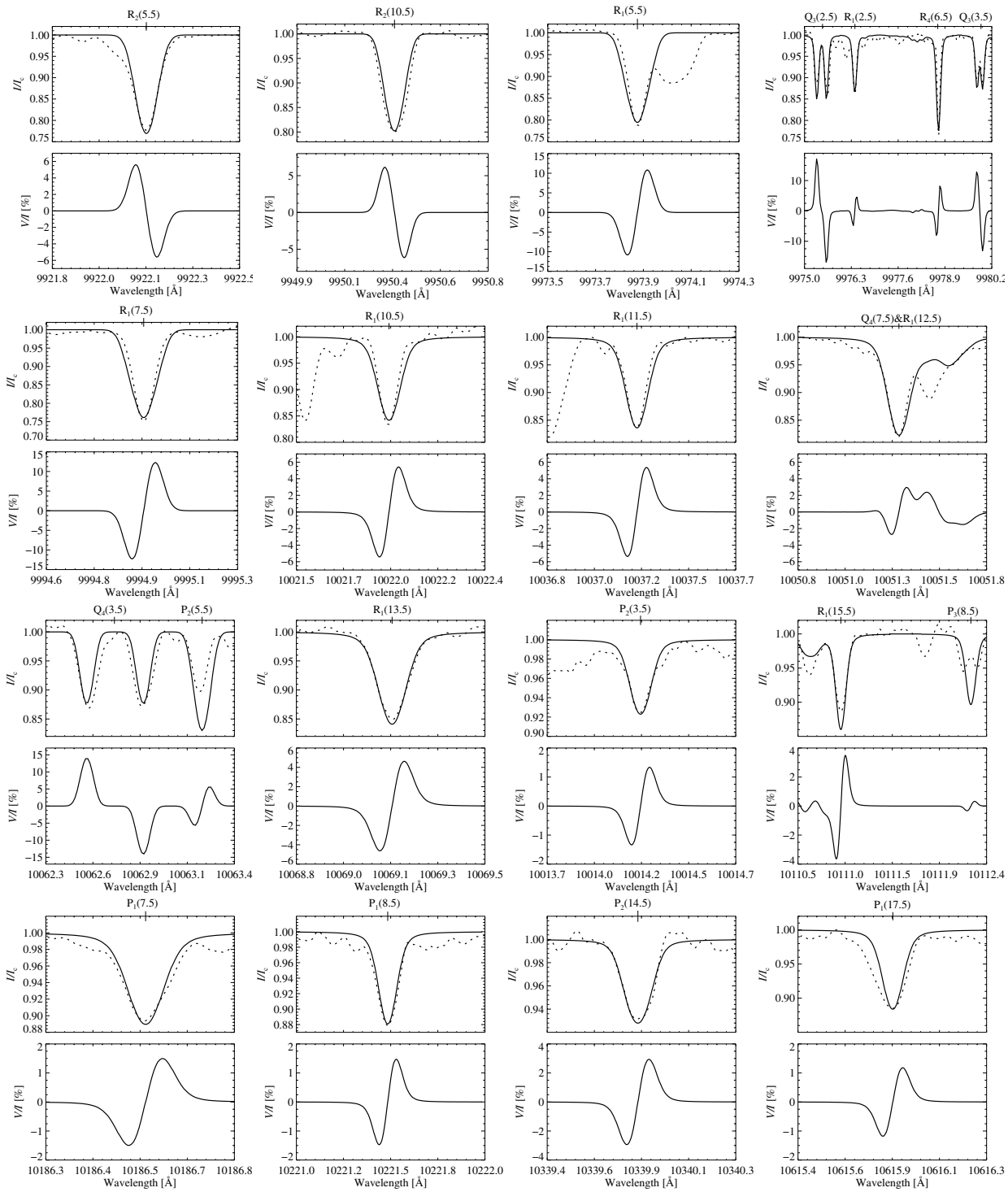

Fig. 2. Zeeman broadening of FeH in a sunspot umbra, Stokes I and V (*upper and lower panels* of the respective plots). Observations (dashed, only Stokes I) are from Wallace et al. (1998). Synthetic Stokes profiles (solid) are calculated using constants from Dea03 for a field strength of 3 kG, umbral models with $T_{\rm eff}$ = 4000 K–4500 K (Hauschildt et al. 1999), and filling factors of 0.8–0.99 for the different wavelength regions.

that begin to play a role there are not taken into account sufficiently.

4.2. Perturbed transitions

The spectral synthesis for Stokes I and V using the set of molecular constants provided by Dea03 shows satisfying results for many molecular lines, as can be seen in the previous section. However, we were not able to reproduce all Stokes I profiles rising from the (0, 0) band of the FeH $F^4\Delta$–$X^4\Delta$ system, such as the R_4 and P_4 lines in the atlas of Wallace et al. (1998). Figure 3 illustrates examples of these lines that would be ideally suited for magnetic field diagnostics thanks to their strong splitting and peculiar shapes. These lines with high $\Omega = 3.5$ and $J \gtrsim 10.5$ seem to be affected by an unknown perturbation. The Hamiltonian provided by Dea03 does not take into account well enough the dependence on the quantum number Ω and the rotational number J to be able to reproduce the intensity profiles

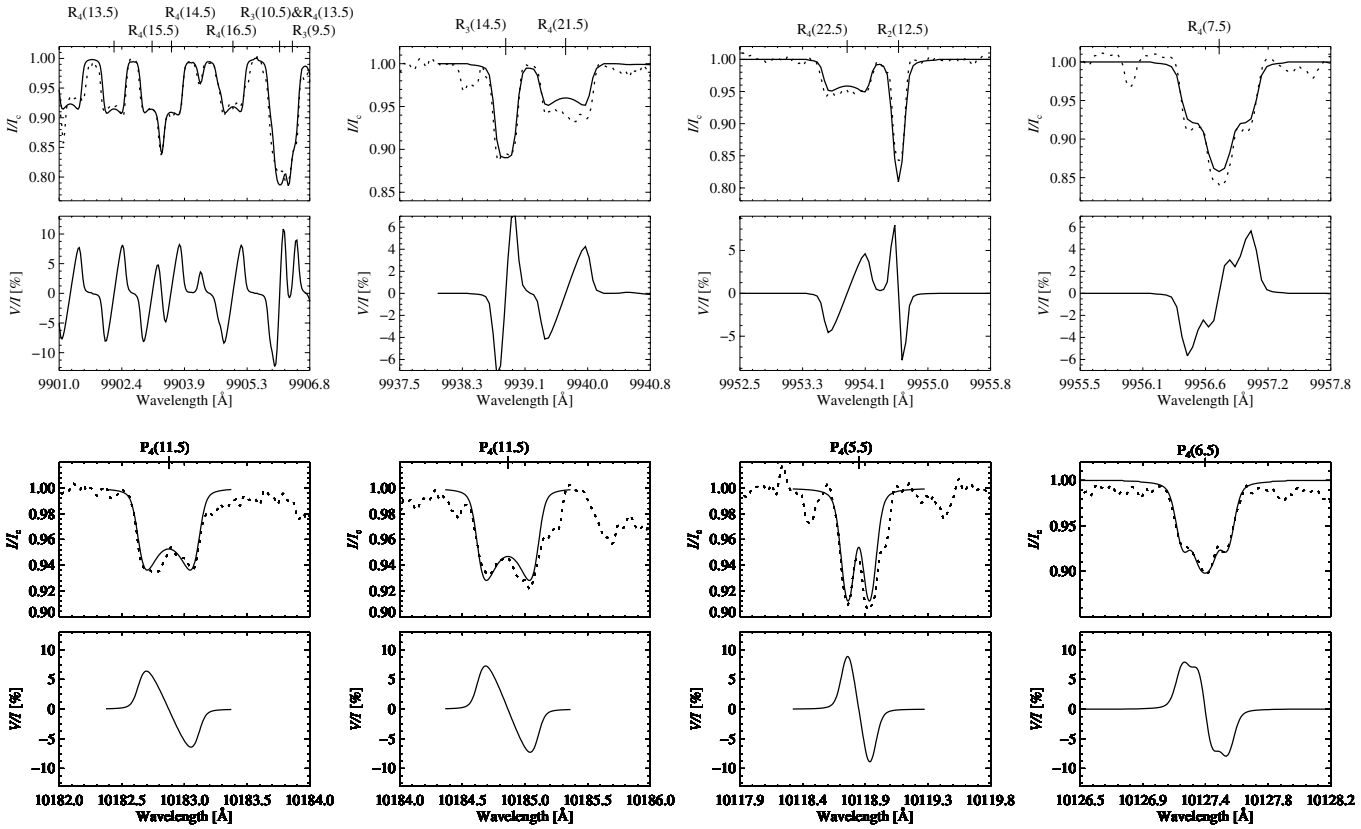

Fig. 3. The same as Fig. 2 but with synthetic profiles calculated using empirical spin-orbit constants A. The field strength of 3 kG, umbral models with $T_{\rm eff}$ = 4000 K–4300 K, and filling factors of 0.8–0.95 were used. In Afram et al. (2007) it is shown how the constants from Dea03 lead to a poor fit for the top left wavelength region as an example.

properly (see Fig. 3 in Afram et al. 2007). For those transitions we searched for spin-orbit interaction constants A to obtain best fits to the observed spectral lines, as described in the introduction of this section. The fits are also shown in Fig. 3.

In addition to the (0, 0) band of the FeH $F^4\Delta$–$X^4\Delta$ system, we found empirical molecular constants for the R_1 and R_2 lines of the (0, 1) band observed farther into the infrared. In Fig. 4 we present Stokes I and V profiles of the (0, 1) band and compare them with synthetic profiles. Stokes I and V observations were obtained by Rüedi et al. (1995) and at the VTT. The spectropolarimetric observations provide important additional constraints for the sign of the effective Landé factors, which would remain inaccessible by intensity measurements alone.

5. Landé factors

5.1. Landé factors of energy levels

The Landé factors of M sublevels of the energy levels of FeH can be calculated according to Eq. (2) as

$$g = \frac{M\Delta\sigma_0}{\Delta E}\,. \tag{6}$$

In the Zeeman regime, which is applicable to the FeH transitions observed in sunspots, the Landé factors for M sublevels are the same for the same J. Since the ratio of spin-orbit coupling to the rotational constant $Y'' \approx 18$ for the $X^4\Delta$-state and $Y' \approx 21$ for the $F^4\Delta$-state, the Landé factor for both states should take the form of case (a) for $J \lesssim 3.5$, and they should approach case (b) for $J \gtrsim 20.5$, while for $3.5 \lesssim J \lesssim 20.5$ the intermediate case is appropriate. In Fig. 5 we have plotted the best-fit Landé factors $g'_{\rm f}$ and $g''_{\rm f}$ of the upper and lower J levels, respectively, within the quartet states of FeH. We also obtained polynomial fits to those measurements in the form

$$g_{\rm f} = C_0 + \frac{C_1}{J(J+1)} + \frac{C_2}{[J(J+1)]^2}, \tag{7}$$

taking the $1/[J(J+1)]$ dependence of the Landé factor into account. The polynomial coefficients C_i for the upper and lower states are given in Table 1. The values of the Landé factors obtained with the polynomial fits are given in Table 2. The intermediate Landé factors preferably lie between the Landé factors for Hund's cases (a) and (b). In Fig. 6 we plot the absolute values of the weighted differences between the best-fit Landé factors $g_{\rm f}$ and the the Landé factors for the intermediate case (a–b) gi, which were calculated using the Hamiltonian from Dea03. The differences are weighted with the rotational number J following Eqs. (8)–(10) to demonstrate the qualitative increase of deviations, leading to a considerable difference in splitting for higher J.

It is interesting to compare our results with those by Brown et al. (2006), who determined the Landé factors of a few energy levels with high accuracy from laboratory measurements for the FeH $X^4\Delta$ state with $J < 7.5$. They could not analyze the upper state and higher rotational numbers since this exceeds the limits of laboratory measurements. We find good agreement within our error bars (see Fig. 5), although the two analyses differ in approaches and are based on completely different experimental data: on one hand, sunspot observations and laboratory measurements on the other. This strengthens our confidence in

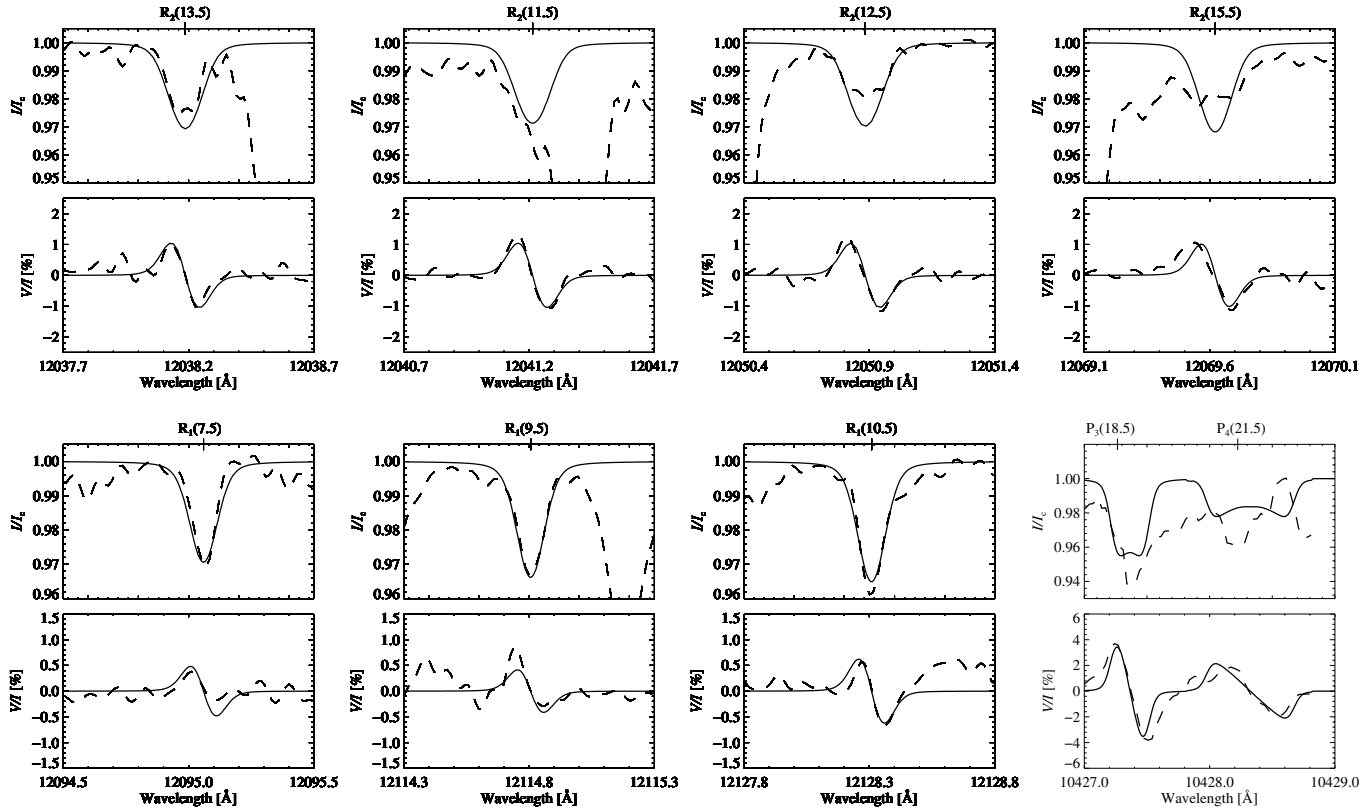

Fig. 4. FeH Stokes I and Stokes V line profiles (*upper and lower panels* respectively). Solid lines represent synthetic Stokes profiles, calculated to fit observed Stokes I and V profiles (dashed lines) from sunspot observations from Rüedi et al. (1995) (0–1 band) and from the VTT (lowest right, 0–0 band). Synthetic profiles were calculated with empirical spin-orbit constants A, with a field strength of 3 kG, an umbral model with $T_{\rm eff}$ = 4800 K (4500 K for the VTT observation), and a filling factor of 0.80.

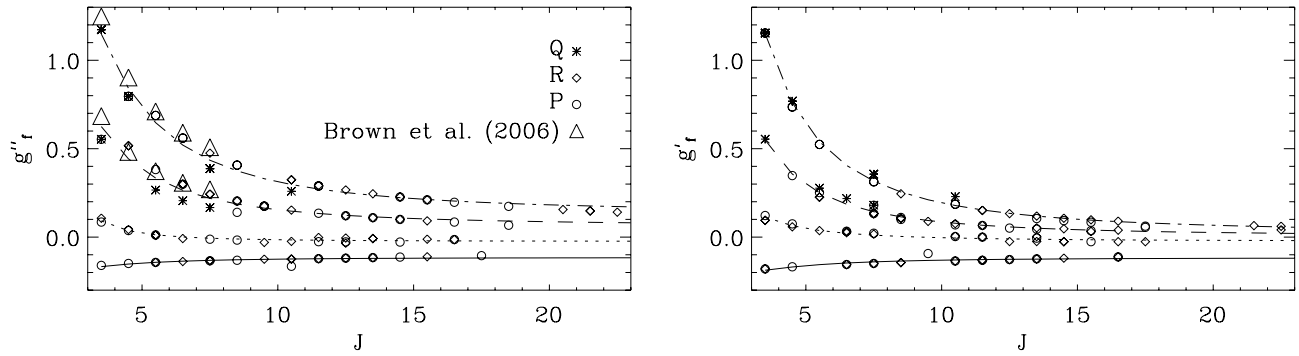

Fig. 5. The best-fit Landé factors for intermediate case (a, b) of the lower ($g''_{\rm f}$) and upper ($g'_{\rm f}$) levels of the quartet states of FeH. Symbols indicate the measurements obtained by fitting to spectral line profiles, and the dashed-dotted, dashed, dotted, and solid lines show the polynomial fit to the measurements for $\Omega = \frac{7}{2}, \frac{5}{2}, \frac{3}{2}$, and $\frac{1}{2}$ respectively. The coefficients for the fits are given in Table 1.

the Landé factors of levels with higher rotational numbers and proves once more the importance of solar data for high-energy molecular spectroscopy.

5.2. Landé factors of transitions

In addition to the Landé factors of the J levels, we used the best fits to the Stokes profiles to extract the best-fit effective Landé factors of numerous transitions in the Q, R, and P branches (with $\Delta J = 0, +1, -1$, respectively) between electronic states with different Ω from our perturbation calculation. These are plotted in Fig. 7 with various symbols. On the other hand, the effective Landé factors can also be obtained from the level Landé factors. According to Berdyugina et al. (2003, 2005), they can be expressed as

$$2g_{\rm eff}(R) = g'(J'+1) - g''J'', \tag{8}$$

$$2g_{\rm eff}(Q) = g' + g'', \tag{9}$$

$$2g_{\rm eff}(P) = -g'J' + g''(J''+1). \tag{10}$$

Using these expressions and the values of $g'_{\rm f}$ and $g''_{\rm f}$ obtained in the previous section with the polynomial fits, we calculated analogous fits to the effective Landé factors. These are shown in Fig. 7 with lines and listed in Table 3 for selected J numbers. The good fit of the curves to the directly measured values suggest that there is no systematic bias inherent in either approach.

Table 1. Polynomial coefficients for Eq. (7).

Coefficient		g'				g''		
	$\Omega = 1/2$	3/2	5/2	7/2	1/2	3/2	5/2	7/2
C_0	−0.116283	−0.0234703	0.00472052	0.0215877	−0.114846	−0.0248106	0.0623232	0.134884
C_1	−1.63587	2.20951	8.96560	19.1359	−1.13826	0.959292	10.3752	20.1569
C_2	8.12147	−0.902763	−6.21278	−21.3215	5.05882	13.7502	−23.8621	−66.0804

Table 2. Upper and lower state Landé factors g' and g'' obtained from polynomial approximations to measurements.

J		g'				g''		
	$\Omega = 1/2$	3/2	5/2	7/2	1/2	3/2	5/2	7/2
3.5	−0.187	0.113	0.549	1.151	−0.167	0.092	0.625	1.148
4.5	−0.169	0.064	0.357	0.760	−0.153	0.036	0.443	0.841
5.5	−0.156	0.038	0.251	0.540	−0.143	0.013	0.334	0.647
6.5	−0.146	0.021	0.186	0.405	−0.136	0.001	0.265	0.521
7.5	−0.140	0.011	0.144	0.317	−0.131	−0.006	0.219	0.435
8.5	−0.135	0.004	0.115	0.255	−0.128	−0.011	0.187	0.374
9.5	−0.132	−0.001	0.094	0.211	−0.126	−0.014	0.164	0.330
10.5	−0.129	−0.005	0.079	0.179	−0.124	−0.016	0.147	0.297
11.5	−0.127	−0.008	0.067	0.154	−0.123	−0.017	0.133	0.272
12.5	−0.126	−0.010	0.058	0.134	−0.121	−0.019	0.123	0.252
13.5	−0.124	−0.012	0.050	0.119	−0.120	−0.020	0.115	0.236
14.5	−0.123	−0.014	0.044	0.106	−0.120	−0.020	0.108	0.223
15.5	−0.123	−0.015	0.040	0.096	−0.119	−0.021	0.103	0.213
16.5	−0.122	−0.016	0.036	0.088	−0.119	−0.021	0.098	0.204
17.5	−0.121	−0.017	0.032	0.080	−0.118	−0.022	0.094	0.197
18.5	−0.121	−0.017	0.030	0.074	−0.118	−0.022	0.091	0.190
19.5	−0.120	−0.018	0.027	0.069	−0.118	−0.022	0.088	0.185
20.5	−0.120	−0.018	0.025	0.065	−0.117	−0.023	0.086	0.180
21.5	−0.120	−0.019	0.023	0.061	−0.117	−0.023	0.084	0.176
22.5	−0.119	−0.019	0.022	0.058	−0.117	−0.023	0.082	0.172
23.5	−0.119	−0.020	0.020	0.055	−0.117	−0.023	0.080	0.170
24.5	−0.119	−0.020	0.019	0.052	−0.117	−0.023	0.079	0.167
25.5	−0.119	−0.020	0.018	0.050	−0.116	−0.023	0.078	0.165

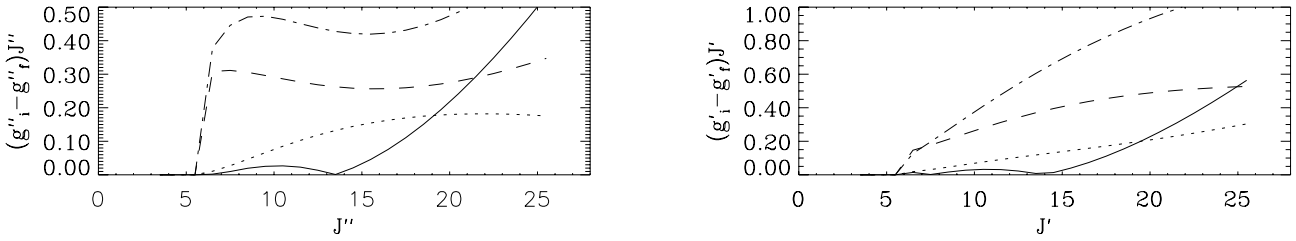

Fig. 6. With J-weighted differences between the best-fit Landé factors (g''_f and g'_f, for the lower and upper levels of the quartet states of FeH, respectively) and the Landé factor for the intermediate case (a, b) g_i using the Hamiltonian from Dea03. The dashed-dotted, dashed, dotted, and solid lines correspond to $\Omega = \frac{7}{2}, \frac{5}{2}, \frac{3}{2}$, and $\frac{1}{2}$ respectively.

6. FeH in red and brown dwarfs

Valenti et al. (2001) pointed out the importance of FeH for the study of magnetic fields on red and brown dwarfs, since it persists to temperatures where atomic diagnostics vanish. Another advantage of using FeH as a Zeeman diagnostic for M and L dwarfs is that many lines of the same species exist in a relatively narrow wavelength region and are only moderately blended.

Recently, Reiners & Basri (2006) used the method of Valenti et al. (2001) for measuring magnetic fields on cool stars with FeH transitions. They showed that the FeH features can distinguish between negligible, moderate, and high magnetic fluxes on low-mass stars (with an accuracy of ∼1 kG). The method is based on a comparison between the spectrum of a star with unknown magnetic field strength and spectra of stars for which the magnetic field strengths can be calibrated in atomic lines.

To demonstrate the magnetic sensitivity of lines of the FeH $F^4\Delta$–$X^4\Delta$ system, we carried out calculations of Stokes I and V profiles of the highly magnetically sensitive R_4 lines around 9900 Å for a sunspot model at different magnetic field strengths using the best-fit Landé factors. The result is shown in Fig. 8: one can see the development of the synthetic profiles to the characteristic, almost rectangular, Stokes I profiles, as compared with observations by Wallace et al. (1998). Along with the FeH lines, the employed line list includes a number of weak atomic lines. Using Dea03's values for the spin-orbit constant A these characteristic profiles cannot be reproduced.

To analyze the potential of FeH as a brown dwarf diagnostic, we used a model assuming a spot contribution of 10% of the

Table 3. The approximated effective Landé factors for selected J numbers.

Branch	J	$\Omega = 1/2$	3/2	5/2	7/2
Q	3.5			0.55	1.16
	8.5			0.15	0.31
	13.5			0.09	0.19
	18.5			0.07	0.15
	23.5			0.06	0.13
R	5.5	0.19	0.04	0.27	0.48
	10.5	0.15	0.02	0.34	0.69
	15.5	0.13	0.06	0.41	0.83
	20.5	0.12	0.10	0.48	0.97
	25.5	0.11	0.12	0.52	1.05
P	5.5	0.09	0.17	0.41	0.50
	8.5	0.10	0.16	0.43	0.85
	13.5	0.12	0.14	0.41	1.00
	18.5	0.14	0.14	0.43	1.16
	23.5	0.15	0.14	0.46	1.34

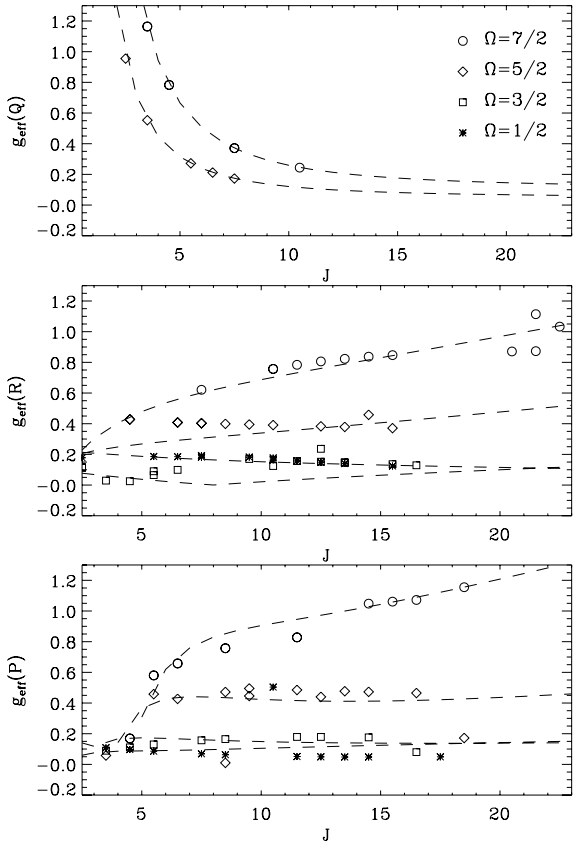

Fig. 7. The best-fit effective Landé factors (symbols) and approximated values with Eqs. (8)–(10) (lines).

stellar disc and a spot comprising only longitudinal magnetic fields and estimated the strength of the Stokes V signal in the FeH lines that could be expected to be observed from starspots. We modeled a cool photosphere with a magnetic field of B = 3 kG to calculate the Stokes V signal for FeH and obtained a maximum signal of ~1.5% (Fig. 9), which was reduced down to ~0.5% when a vsini of 10 km s^{-1} was applied. This promises the direct detection of magnetic fields on ultracool stars.

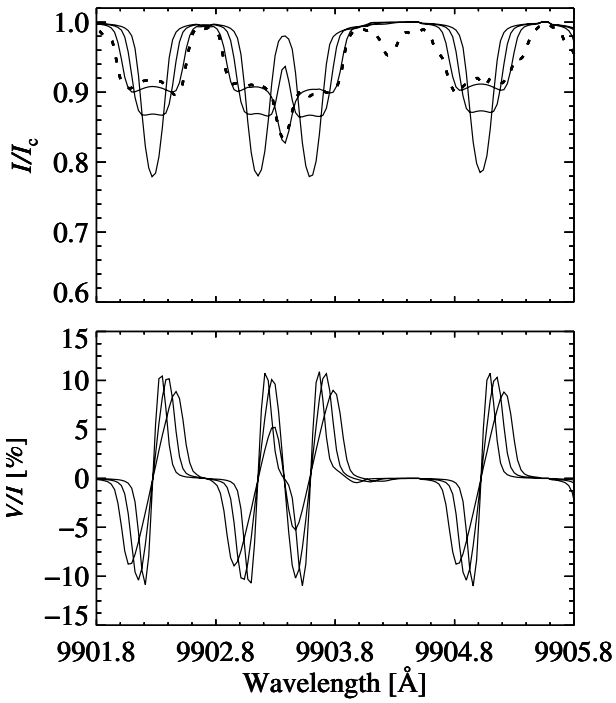

Fig. 8. Stokes I and V profiles of the FeH R_4 lines around 9900 Å calculated for field strengths of 1.0, 2.0, and 3.0 kG, an umbral model with $T_{\rm eff}$ = 4300 K (Hauschildt et al. 1999), for a filling factor of 0.98 (solid lines). The dashed line is the sunspot observation by Wallace et al. (1998).

7. Conclusions

Observations of the FeH $F^4\Delta$–$X^4\Delta$ system and their successful modeling open an opportunity for fully exploiting the diagnostic capabilities of this molecular system, which represents a powerful tool for solar and stellar magnetic field studies.

Our goal was to determine the Landé factors of the levels and transitions for the FeH $F^4\Delta$–$X^4\Delta$ system, which characterize the magnetic sensitivity of the spectral lines of that system and, thus, provide us with a magnetic diagnostic tool. For this purpose we have described the synthesis of molecular Stokes parameters and shown that it is possible to fit a wide range of available spectral lines in different wavelength regions with various ΔJ, J, and Ω numbers with the set of molecular constants provided by Dea03, especially lines with small J numbers. Nevertheless, interesting spectral regions exist, such as the region around 9900 Å, where a strong splitting is observed that cannot be modeled with the available constants. To employ the advantages offered by such lines, we developed a semi-empirical model with modified spin-orbital constants and were able to reproduce strongly split Stokes I and Stokes V profiles observed in sunspot spectra. More important, however, was the extraction of the Landé factors of levels and transitions obtained from this fitting procedure. In contrast to laboratory measurements, a determination of the Landé factors of levels is possible for the ground, as well as for the excited state, and also for high rotational numbers. Calculations based on the applied perturbation theory with the Hamiltonian provided by Dea03 could perfectly reproduce observations of the effective Landé factors for the Q branch (i.e. $\Delta J = 0$) of this transition, while the R and P branches cannot be treated in the same way because of the existence of an unknown perturbation, leading to the necessary modifications of the spin-orbit constant.

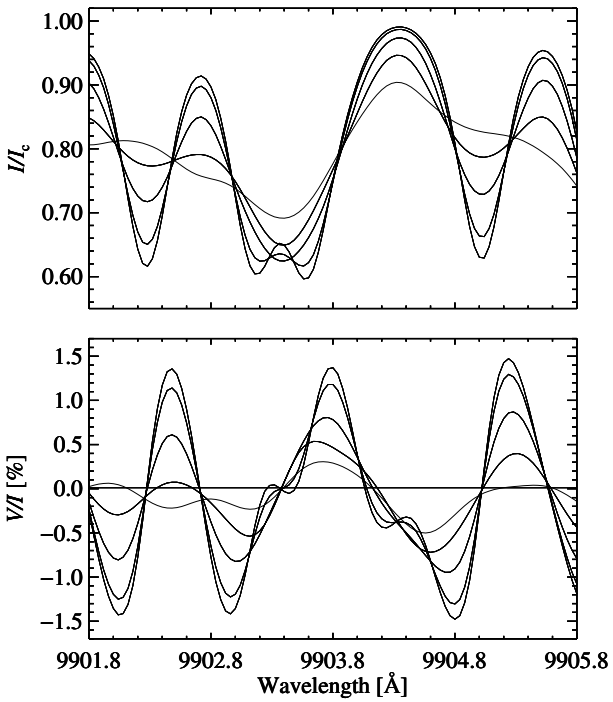

Fig. 9. Stokes *I* and *V* for a model star with 10% longitudinal magnetic field of 3 kG, with a photosphere temperature of 3400 K, and with a spot temperature of 3000 K. The development of the profiles with increasing vsini from 0 km s^{-1} to 20 km s^{-1} with a step of 5 km s^{-1} is shown.

We conclude that our ability to model the FeH $F^4\Delta$–$X^4\Delta$ system based on a set of theoretical and empirical molecular constants provides a new valuable source of information about the physical parameters in cool objects.

For the detection of magnetic fields on brown dwarfs, we calculated expected Stokes *V* signals in sensitive FeH lines and obtained a maximum signal of about 1.5%, confirming FeH as an excellent tool for obtaining information on the magnetic fields on L-type stars, and thus for gaining insight into their dynamo processes.

Acknowledgements. We acknowledge the EURYI award from the ESF, the SNF grants PE002-104552 and 200021-103696, and the ETH Research Grant TH-2/04-3. We are thankful to P. Hauschildt for providing model atmospheres.

References

Afram, N., Berdyugina, S. V., Fluri, D. M., et al. 2007, A&A, 473, L1
Berdyugina, S. V., & Solanki, S. K. 2002, A&A, 385, 701
Berdyugina, S. V., Frutiger, C., Solanki, S. K., & Livingston, W. 2000, A&A, 364, L101
Berdyugina, S. V., Solanki, S. K., & Frutiger, C. 2001, in Magnetic Fields Across the Hertzsprung-Russell Diagram, ed. G. Mathys, S. K. Solanki, & D. T. Wickramasinghe, ASP Conf. Ser., 248, 9
Berdyugina, S. V., Solanki, S. K., & Frutiger, C. 2003, A&A, 412, 513
Berdyugina, S. V., Braun, P. A., Fluri, D. M., & Solanki, S. K. 2005, A&A, 444, 947
Brown, J. M., Körsgen, H., Beaton, S. P., & Evenson, K. M. 2006, J. Chem. Phys., 124, 234309
Dulick, M., Bauschlicher Jr., C. W., Burrows, A., et al. 2003, ApJ, 594, 651
Frutiger, C., Solanki, S. K., Fligge, M., & Bruls, J. H. M. J. 2000, A&A, 358, 1109
Hauschildt, P. H., Allard, F., & Baron, E. 1999, ApJ, 512, 377
Mártinez Pillet, V., Collados, M., Sánchez Almeida, J., et al. 1999, in High Resolution Solar Physics: Theory, Observations, and Techniques, ed. T. R. Rimmele, K. S. Balasubramaniam, & R. R. Radick, ASP Conf. Ser., 183, 264
Phillips, J. G., Davis, S., Lindgren, B., & Balfour, W. J. 1987, ApJS, 65, 721
Reiners, A., & Basri, G. 2006, ApJ, 644, 497
Rüedi, I., Solanki, S. K., Livingston, W., & Harvey, J. 1995, A&A, 113, 91
Solanki, S. K. 1987, Ph.D. Thesis, ETH, Zurich, Switzerland
Solanki, S. K., Rüedi, I., & Livingston, W. 1992, A&A, 263, 312
Valenti, J. A., Johns-Krull, C. M., & Piskunov, N. E. 2001, in 11th Cool Stars, Stellar Systems and the Sun, ed. R. J. García López, R. Rebolo, & M. R. Zapatero Osorio, ASP Conf. Ser., 223, 1579
Wallace, L., Livingston, W. C., Bernath, P. F., & Ram, R. S. 1998, An Atlas of the Sunspot Umbral Spectrum in the Red and Infrared from 8900 to 15 050 cm^{-1} (6642 to 11 230 Å) (NOAO)